

Dissipation-Assisted Prethermalization in Long-Range Interacting Atomic Ensembles

Stefan Schütz, Simon B. Jäger, and Giovanna Morigi

Theoretische Physik, Universität des Saarlandes, D-66123 Saarbrücken, Germany

(Received 16 December 2015; revised manuscript received 11 May 2016; published 15 August 2016)

We theoretically characterize the semiclassical dynamics of an ensemble of atoms after a sudden quench across a driven-dissipative second-order phase transition. The atoms are driven by a laser and interact via conservative and dissipative long-range forces mediated by the photons of a single-mode cavity. These forces can cool the motion and, above a threshold value of the laser intensity, induce spatial ordering. We show that the relaxation dynamics following the quench exhibits a long prethermalizing behavior which is first dominated by coherent long-range forces and then by their interplay with dissipation. Remarkably, dissipation-assisted prethermalization is orders of magnitude longer than prethermalization due to the coherent dynamics. We show that it is associated with the creation of momentum-position correlations, which remain nonzero for even longer times than mean-field predicts. This implies that cavity cooling of an atomic ensemble into the self-organized phase can require longer time scales than the typical experimental duration. In general, these results demonstrate that noise and dissipation can substantially slow down the onset of thermalization in long-range interacting many-body systems.

DOI: [10.1103/PhysRevLett.117.083001](https://doi.org/10.1103/PhysRevLett.117.083001)

The quest for a systematic understanding of non-equilibrium phenomena is an open problem in theoretical physics for its importance in the description of dynamics from the microscopic up to astrophysical scales [1–3]. Aspects of these dynamics are studied in the relaxation of systems undergoing temporal changes (quenches) of the control field across a critical point [4–6]. Quenches across a nonequilibrium phase transition provide further insight into the interplay between noise and external drives on criticality and thermalization [7,8]. In this context, photonic systems play a prominent role, thanks to their versatility [9–15].

Polarizable particles in a high-finesse cavity, like in the setup illustrated in Fig. 1(a), offer a unique system to study relaxation in long-range interacting systems. Here, multiple photon scattering mediates particle-particle interactions whose range scales with the system size in a single-mode cavity [15–18]. In this limit, atomic ensembles in cavities are expected to share several features with other long-range interacting systems such as gravitational clusters and non-neutral plasmas in two or more dimensions [3,16,19]. The equilibrium thermodynamics of these systems can exhibit ensemble inequivalence [3,20], while quasistationary states (QSSs) typically characterize the out-of-equilibrium dynamics [3,21–23]. QSSs are metastable states in which the system is expected to remain trapped in the thermodynamic limit; they are Vlasov-stable solutions and thus depend on the initial state. So far, however, evidence of QSSs has been elusive. It has been conjectured that noise and dissipation can set a time scale that limits the QSS lifetime [24–27] and possibly gives rise to dynamical phase transitions [25]. In Ref. [28], it was shown that, in the presence of dissipation due to viscous damping or local

inelastic collisions, the relaxation dynamics of long-range interacting systems can be cast in terms of so-called scaling QSSs, which are solutions of the kinetic mean-field equation and asymptotically tend to a unique QSS [28]. Accordingly, one would expect to observe QSSs in cavity systems [19]. In Ref. [16], however, we found no evidence of the typical superlinear dependence on N of the QSS time scale [3], which we attributed to the effect of noise and dissipative processes. Nonetheless, the dissipative dynamics is here due to retardation effects in the coupling between the atoms and a global variable, the cavity field, and can also establish long-range correlations [29,30] whose influence on the relaxation dynamics is still unexplored.

In this work, we characterize the interplay between dissipative and conservative long-range forces in the semiclassical dynamics of N polarizable particles (atoms) confined within a high-finesse single-mode cavity and transversally driven by a laser [16,31–33] [see Fig. 1(a)]. The particles' motion is along the cavity axis (x axis), and the dynamics results from their optomechanical coupling with the cavity mode at wave number k and spatial mode function $\cos(kx)$. We focus on the regime where the laser frequency ω_L is smaller than the cavity frequency ω_c , such that $\Delta_c = \omega_L - \omega_c < 0$. Here, the dynamics is characterized by a thermal stationary state, which can exhibit a second-order driven-dissipative phase transition (spatial self-organization) as a function of the laser intensity and of Δ_c [31]. This transition is due to the interplay between the dispersive and the dissipative forces: The dispersive forces tend to order the atoms in gratings for which the order parameter $\Theta = \sum_{j=1}^N \cos(kx_j)/N \rightarrow \pm 1$, with x_j the particles' positions, and the intracavity photon number is maximum. The dissipative forces, instead, are due to

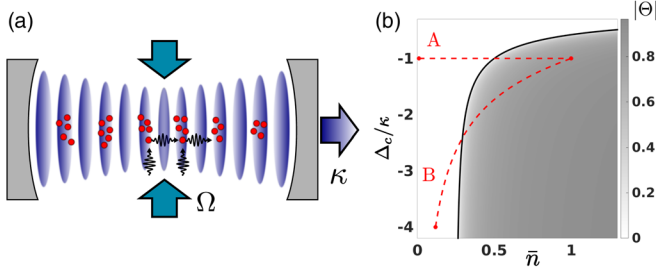


FIG. 1. (a) Atoms interact with the standing-wave mode of a cavity and are transversally driven by a laser. The laser amplitude (Ω) and/or frequency (Δ_c) are suddenly quenched across the threshold, above which the atoms organize in regular spatial patterns at the steady state. The coherent scattering amplitude per atom, S , is tuned by the laser, $S \propto \Omega$, and the resonator dissipates photons at rate κ . (b) Phase diagram of the second-order self-organization transition as a function of \bar{n} (proportional to S^2) and Δ_c/κ (that determines the asymptotic temperature). The black line separates the homogeneous phase (with order parameter $\Theta = 0$) from the self-organized one (with $\Theta \rightarrow \pm 1$). The red dashed lines A and B illustrate the initial and final values, respectively, of the sudden quenches we analyze.

retardation effects in the dynamics of atoms and field: For $\Delta_c < 0$, they cool the atoms into a thermal state whose effective temperature T_{eff} is determined by Δ_c and by the cavity loss rate κ : $k_B T_{\text{eff}} = \hbar(\Delta_c^2 + \kappa^2)/(-4\Delta_c)$, with k_B the Boltzmann constant [30–32,34–37]. T_{eff} determines the threshold S_c of the coherent laser scattering amplitude S per atom at which spatial self-organization occurs, such that $\sqrt{N}S_c = 2k_B T_{\text{eff}}/\hbar$ [31,34,38], and separates the regime where the spatial distribution is uniform and $\Theta \simeq 0$ from the symmetry broken phase in which the atoms form Bragg gratings, as shown in Fig. 1(b).

We analyze the semiclassical dynamics of the atoms after a quench across the transition using a Fokker-Planck equation (FPE) for the phase space distribution $f(x_1, \dots, x_N; p_1, \dots, p_N; t)$ at time t and as a function of the atoms' positions x_j and the momenta p_j . The FPE is valid when the cavity linewidth κ exceeds the recoil frequency $\omega_r = \hbar k^2/(2m)$ and the width of the momentum distribution Δp is larger than the photon linear momentum $\hbar k$ [30]. It reads [31,39]

$$\partial_t f = \{H, f\} + \bar{n} \mathcal{L}_\beta f + O(U_0), \quad (1)$$

where Hamiltonian $H = \sum_{j=1}^N p_j^2/(2m) + \hbar \Delta_c \bar{n} N \Theta^2$ determines the coherent dynamics and is a realization of the anisotropic Hamiltonian Mean Field model (HMF) [16,21,40]. The dimensionless parameter $\bar{n} = NS^2/(\kappa^2 + \Delta_c^2)$ scales the depth of the conservative potential. It also scales the dissipator \mathcal{L}_β , describing the effective long-ranged friction and diffusion [30,31]:

$$\mathcal{L}_\beta f = \sum_i^N \frac{\Gamma}{N} \sum_j^N \sin(kx_i) \partial_{p_i} \sin(kx_j) \left(p_j + \frac{m}{\beta} \partial_{p_j} \right) f, \quad (2)$$

with $\Gamma = 2\omega_r \hbar \kappa \beta$ and $\beta = (k_B T_{\text{eff}})^{-1}$. For $\Delta_c < 0$, the incoherent dynamics drives the system into the stationary state $f_S(\beta, \bar{n}) = f_0 \exp(-\beta H)$, where f_0 warrants normalization. This state is well defined in the thermodynamic limit we choose, according to which, as N is increased, the quantity NS^2 (and thus \bar{n}) is kept constant. This choice warrants that the Hamiltonian satisfies Kac's scaling [3].

The relaxation dynamics following a sudden quench at $t = 0$ is numerically evaluated by means of stochastic differential equations (SDE). Averages are taken over several trajectories, sampling the dynamics of N atoms according to the given initial distribution [30,41]. Before the quench is performed ($t < 0$), we assume that the system has reached the equilibrium solution $f_S(\beta, \bar{n}_i)$ of the FPE at a given value of $\bar{n} = \bar{n}_i$ and Δ_c . At $t = 0$, the value of \bar{n} is quenched from $\bar{n}_i < \bar{n}_c$, deep in the disordered phase, to $\bar{n}_f > \bar{n}_c$, well inside the ordered phase. This corresponds to the horizontal path A of Fig. 1(b), keeping Δ_c , and hence the asymptotic temperature, constant. We evolve the initial state setting $\bar{n} = \bar{n}_f$ in Eq. (1). In what follows, we focus on quenches from the disordered to the ordered phase along path A; nevertheless, the essential features of the dynamics we will report on characterize also the quenches in the opposite direction as well as along paths of type B, which connects points with different asymptotic temperatures (see Supplemental Material [42]).

The time evolution of the modulus of the order parameter $\langle |\Theta| \rangle$ is displayed in Fig. 2(a) for different values of \bar{n}_f : $\langle |\Theta| \rangle$ tends towards an asymptotic value that is closer to unity the larger is \bar{n}_f . Before reaching the steady state, the dynamics go through different stages, which we classify as follows: (i) A fast relaxation towards an intermediate value of the magnetization with time scale $t \lesssim 10^2 \kappa^{-1}$; this time scale decreases with \bar{n}_f . (ii) A transient regime where $\langle |\Theta| \rangle$ seems to grow logarithmically with time. (iii) Finally, the dissipation becomes dominant and brings the system to the asymptotic value, which is exponentially approached over time scales of the order of $10^6 \kappa^{-1}$. These time scales are illustrated in Fig. 2(a) and here reported for $N = 50$ particles but generally depend on N , as we discuss later on.

We first observe that, being Δ_c negative, the growth of $\langle |\Theta| \rangle$ [Fig. 2(a)] corresponds to a monotonic decrease of the potential energy, $V = \hbar \Delta_c \bar{n} N \Theta^2$. In the fast relaxation stage (i), this decrease is well fitted by an exponential and is associated with a corresponding decrease of the relative fluctuations (see the inset), indicating that the cavity field exponentially grows and creates a mechanical potential, which increasingly localizes the atoms at its minima. The exponential potential depth growth is due to this

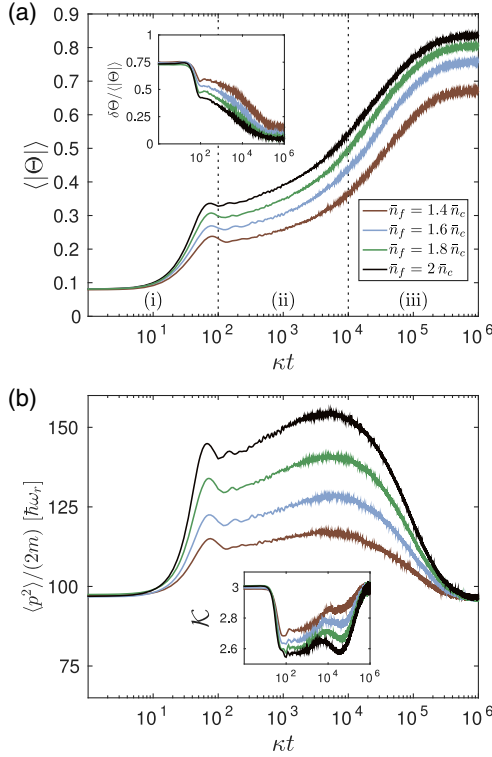


FIG. 2. Numerical simulation of the dynamics following a sudden quench along path A using the SDE [31]. At $t = 0$, the atoms are in the stationary state of Eq. (1) for $\bar{n}_i = 0.01\bar{n}_c$ with $\Delta_c = -\kappa$, and \bar{n} is quenched to the value $\bar{n}_f > \bar{n}_c$ [see the legend in (a)]. (a) The modulus of the order parameter $\langle |\Theta| \rangle$ and (b) the single-particle kinetic energy $\langle p^2 \rangle / (2m)$ (in units of $\hbar\omega_r$) as a function of time (in units of κ^{-1}) for $N = 50$. The corresponding insets display the time evolution of the relative localization $\delta\Theta / \langle |\Theta| \rangle$, where $\delta\Theta = \sqrt{\langle \Theta^2 \rangle - \langle |\Theta| \rangle^2}$, and of the kurtosis \mathcal{K} . The initial values $\langle |\Theta| \rangle_{t=0} \approx 1/\sqrt{\pi N} \approx 0.08$ in (a) are due to finite N [31]. Here, $\kappa \approx 390\omega_r$ and $N|U_0| = 0.05\kappa$. The three relaxation stages are indicated by the labels (i), (ii), and (iii).

nonlinearity: The more the atoms become localized in the Bragg grating, the larger is the scattering amplitude and, thus, the potential depth. The increasing localization correspondingly augments the kinetic energy, as visible in Fig. 2(b). In this regime, thus, the total energy is conserved, and the dynamics is coherent and consists in a transfer of energy from spatial into momentum fluctuations. Correspondingly, the single-particle momentum distribution becomes increasingly nonthermal, as visible by inspecting the time evolution of the kurtosis, $\mathcal{K} = \langle p^4 \rangle / \langle p^2 \rangle^2$, shown in the inset in Fig. 2(b): \mathcal{K} exponentially deviates from the value of the initial Gaussian (“thermal”) state, for which $\mathcal{K}_{\text{gauss}} = 3$. We have verified that this dynamics is well described by a Vlasov equation for the single-particle distribution $f_1(x, p; t)$, which we derive assuming $f(x_1, \dots, x_N; p_1, \dots, p_N; t) = \prod_{j=1}^N f_1(x_j, p_j; t)$, integrating out the $N - 1$ variables from Eq. (1) for the initial uniform distribution and taking the thermodynamic

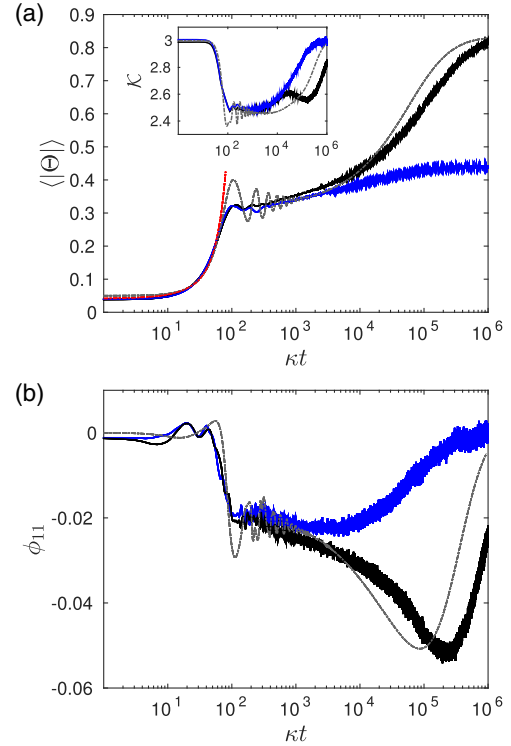


FIG. 3. Dynamics following a sudden quench along path A with $\bar{n}_f = 2\bar{n}_c$ and $N = 200$. At $t = 0$, the atoms are in the stationary state of Eq. (1) for $\bar{n}_i = 0.01\bar{n}_c$ and $\Delta_c = -\kappa$. Subplot (a) compares the evolution of $\langle |\Theta| \rangle$ and \mathcal{K} (inset) obtained by integrating Eq. (1) (black line) with the one found after setting $\Gamma = U_0 = 0$ (blue line). The red line is the fit obtained by a stability analysis of the homogeneous Vlasov solution, the dashed-dotted line by a mean-field model (see Supplemental Material [42]). (b) Time evolution of the QSS observable ϕ_{11} [Eq. (3)] corresponding to the curves in (a).

limit (see Supplemental Material [42] and Ref. [43]). Figure 3(a) compares the result of the FPE with the predictions of the Vlasov equation (red curve), showing an excellent agreement in the fast relaxation regime. Numerical and analytical results show that the time scale of this dynamics depends on N only through the parameter \bar{n} (and is thus constant when Kac’s scaling applies); see also Supplemental Material [42].

After this fast relaxation, the growth in the order parameter and in the kinetic energy seems logarithmic in time. This transient regime (ii) is of Hamiltonian origin: It exhibits damped oscillations, which can be understood as oscillations of the atoms at the minima. Energy is periodically transferred from the kinetic to the potential energy. Since the potential energy depends on a global variable, energy is exchanged between the particles by means of elastic collisions, hence damping the oscillations. Correspondingly, the kurtosis starts to increase towards the Gaussian value, showing that the sample starts to equilibrate. In order to verify this hypothesis, in Fig. 3(a), we compare the predictions of the full simulation (black

curves) for the order parameter and kurtosis with the ones obtained after setting $\Gamma = 0$ in Eq. (1) (blue curves): In the transient regime, the curves nearly overlap for $t \lesssim 10^4 \kappa^{-1}$. Noise and dissipation, however, lead to a discrepancy between the predictions of the Hamiltonian and of the full FPE. This discrepancy becomes increasingly evident at longer time scales: When the dynamics is solely Hamiltonian, in fact, the kurtosis increases monotonically towards the Gaussian value. Because of the analogy with the Hamiltonian dynamics, some of the features of the transient regime are reminiscent of the HMF, where for a similar quench a violent relaxation is observed and then followed by prethermalization in a QSS [21,40]. In our case, for $\Gamma \neq 0$, as in Ref. [16], we do not find evidence of a superlinear scaling with N of the QSS lifetime. The QSS lifetime, in fact, is limited by the dissipative effects, which have the same physical origin as the long-range conservative forces and whose characteristic time scale is linear in N (see Supplemental Material [42] and Ref. [43]). Note that at the end of this stage the atoms are localized, but their temperature is hotter than T_{eff} .

In stage (iii), when the effect of dissipation becomes relevant, the atoms are cooled and further localized at the minima. The kurtosis, however, further decreases till reaching a minimum, before increasing again towards the Gaussian value. We first compare this behavior with the predictions of a mean-field (MF) model, which we extract from Eq. (1) by means of the factorization ansatz; see Supplemental Material [42]. The gray lines in Fig. 3(a) and its inset show the MF predictions as a function of time and indicate that, even though MF reproduces qualitatively the dynamical features, it fails to give the correct time scale by at least one order of magnitude. Further insight is provided by the observable for QSSs [28], which we here define as

$$\phi_{11} = \frac{\langle |\sin(kx)p| \rangle}{\langle |\sin(kx)| \rangle \langle |p| \rangle} - 1. \quad (3)$$

When $\phi_{11} \neq 0$, the distribution is not factorizable into a kinetic and a potential term. Figure 3(b) displays the time evolution of ϕ_{11} for the Hamiltonian, mean-field, and full dynamics. In stages (i) and (ii), the three models predict approximately the same behavior. Instead, in stage (iii), ϕ_{11} evolves differently: For both MF and full FPE it exhibits a minimum, however reached at different times, which seems to possess the features of a scaling QSS, namely, a sequence of QSSs with identical correlations [28]. Its nature could be understood in terms of the onset of collective oscillations which are (almost) decoupled from noise and dissipation. Analogous behaviors have been reported for the case of atomic arrays in a cavity [29,44]. Since the trajectories of ϕ_{11} are different for the three types of simulations, the corresponding QSSs are expected to not be the same. In particular, the discrepancy

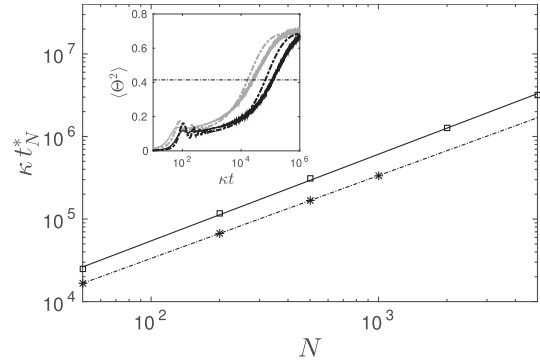


FIG. 4. Relaxation after a sudden quench along path A for the parameters of Fig. 3 ($\bar{n}_f = 2\bar{n}_c$) and for different N . Inset: Time evolution of $\langle \Theta^2 \rangle$ for $N = 50$ (gray) and $N = 200$ (black). The dashed lines are the prediction of the MF model (see Supplemental Material [42]). The horizontal dashed line indicates where $\langle \Theta^2 \rangle$ has reached 60% of its stationary value and identifies the corresponding time t_N^* . Inset: Time t_N^* (in units of κ^{-1}) as a function of N for the full FPE (squares) and MF (stars). The lines are the corresponding linear fits in the log-log plot.

between full FPE and MF in stage (iii) remains of the same order when scaling up the system, while instead Hamiltonian prethermalization tends towards the corresponding mean-field prediction. Figure 4 displays the relaxation time scales for the MF and the full FPE: The two curves suggest a linear increase with N for both cases; nevertheless, they run parallel, thus showing that the discrepancy is a scalable effect. We deduce that this discrepancy is due to the momentum-position correlations due to noise, which are otherwise discarded in the MF treatment.

This prethermalization is not related to the critical slowing down observed in Ref. [45] but is due to the creation of correlations between momentum and position and is reminiscent of kinetic-stop dynamics [46]. It implies that cavity cooling of a large sample of atoms into the self-organized phase, corresponding to a sudden quench along path B, can be very slow and thus inefficient (see also Ref. [34]). Our analysis sets the stage for the development of a kinetic equation that is valid in the full quantum regime [47–51].

We acknowledge discussions with Ralf Betzholtz, Cesare Nardini, and Stefano Ruffo and support by the German Research Foundation (DFG, DACH project “Quantum crystals of matter and light”) and by the German Ministry of Education and Research (BMBF “Q.com”).

-
- [1] T. Chou, K. Mallick, and R. K. P. Zia, *Rep. Prog. Phys.* **74**, 116601 (2011).
 [2] Y. Levin, R. Pakter, F. B. Rizzato, T. N. Teles, and F. P. C. Benetti, *Phys. Rep.* **535**, 1 (2014).

- [3] A. Campa, T. Dauxois, and S. Ruffo, *Phys. Rep.* **480**, 57 (2009).
- [4] P. Calabrese and J. Cardy, *J. Stat. Mech.* (2007) P06008.
- [5] L. Foini, L. F. Cugliandolo, and A. Gambassi, *Phys. Rev. B* **84**, 212404 (2011); F. Iglói and H. Rieger, *Phys. Rev. Lett.* **106**, 035701 (2011).
- [6] A. Polkovnikov, K. Sengupta, A. Silva, and M. Vengalattore, *Rev. Mod. Phys.* **83**, 863 (2011).
- [7] P. C. Hohenberg and B. I. Halperin, *Rev. Mod. Phys.* **49**, 435 (1977); M. C. Cross and P. C. Hohenberg, *Rev. Mod. Phys.* **65**, 851 (1993).
- [8] L. M. Sieberer, M. Buchhold, and S. Diehl, arXiv:1512.00637.
- [9] A. Tomadin and R. Fazio, *J. Opt. Soc. Am. B* **27**, A130 (2010).
- [10] A. Aspuru-Guzik and P. Walther, *Nat. Phys.* **8**, 285 (2012).
- [11] P. Kirton and J. Keeling, *Phys. Rev. Lett.* **111**, 100404 (2013).
- [12] L. J. Zou, D. Marcos, S. Diehl, S. Putz, J. Schmiedmayer, J. Majer, and P. Rabl, *Phys. Rev. Lett.* **113**, 023603 (2014).
- [13] I. Carusotto and C. Ciuti, *Rev. Mod. Phys.* **85**, 299 (2013).
- [14] V. Peano, C. Brendel, M. Schmidt, and F. Marquardt, *Phys. Rev. X* **5**, 031011 (2015).
- [15] H. Ritsch, P. Domokos, F. Brennecke, and T. Esslinger, *Rev. Mod. Phys.* **85**, 553 (2013).
- [16] S. Schütz and G. Morigi, *Phys. Rev. Lett.* **113**, 203002 (2014).
- [17] F. Piazza and H. Ritsch, *Phys. Rev. Lett.* **115**, 163601 (2015).
- [18] E. Tesio, G. R. M. Robb, G.-L. Oppo, P. M. Gomes, T. Ackemann, G. Labeyrie, R. Kaiser, and W. J. Firth, *Phil. Trans. R. Soc. A* **372**, 20140002 (2014).
- [19] R. Bachelard, T. Manos, P. de Buyl, F. Staniscia, F. S. Cataliotti, G. De Ninno, D. Fanelli, and N. Piovella, *J. Stat. Mech.* (2010) P06009.
- [20] I. Latella, A. Pérez-Madrid, A. Campa, L. Casetti, and S. Ruffo, *Phys. Rev. Lett.* **114**, 230601 (2015).
- [21] M. Antoni and S. Ruffo, *Phys. Rev. E* **52**, 2361 (1995).
- [22] A. Gabrielli, M. Joyce, and B. Marcos, *Phys. Rev. Lett.* **105**, 210602 (2010).
- [23] T. M. Rocha Filho, A. E. Santana, M. A. Amato, and A. Figueiredo, *Phys. Rev. E* **90**, 032133 (2014).
- [24] S. Gupta and D. Mukamel, *Phys. Rev. Lett.* **105**, 040602 (2010).
- [25] P.-H. Chavanis, F. Baldovin, and E. Orlandini, *Phys. Rev. E* **83**, 040101 (2011).
- [26] C. Nardini, S. Gupta, S. Ruffo, T. Dauxois, and F. Bouchet, *J. Stat. Mech.* (2012) P12010.
- [27] P. H. Chavanis, *Eur. Phys. J. B* **87**, 120 (2014).
- [28] M. Joyce and T. Worrakitpoonpon, *Phys. Rev. E* **84**, 011139 (2011); M. Joyce, J. Morand, F. Sicard, and P. Viot, *Phys. Rev. Lett.* **112**, 070602 (2014); M. Joyce, J. Morand, and P. Viot, *Phys. Rev. E* **93**, 052129 (2016).
- [29] J. K. Asbóth, P. Domokos, and H. Ritsch, *Phys. Rev. A* **70**, 013414 (2004).
- [30] S. Schütz, H. Habibian, and G. Morigi, *Phys. Rev. A* **88**, 033427 (2013).
- [31] S. Schütz, S. B. Jäger, and G. Morigi, *Phys. Rev. A* **92**, 063808 (2015).
- [32] P. Domokos and H. Ritsch, *Phys. Rev. Lett.* **89**, 253003 (2002).
- [33] A. T. Black, H. W. Chan, and V. Vuletić, *Phys. Rev. Lett.* **91**, 203001 (2003).
- [34] W. Niedenzu, T. Griebner, and H. Ritsch, *Europhys. Lett.* **96**, 43001 (2011).
- [35] P. Horak, G. Hechenblaikner, K. M. Gheri, H. Stecher, and H. Ritsch, *Phys. Rev. Lett.* **79**, 4974 (1997).
- [36] V. Vuletić and S. Chu, *Phys. Rev. Lett.* **84**, 3787 (2000).
- [37] A. Vukics and P. Domokos, *Phys. Rev. A* **72**, 031401(R) (2005).
- [38] J. K. Asbóth, P. Domokos, H. Ritsch, and A. Vukics, *Phys. Rev. A* **72**, 053417 (2005).
- [39] Equation (1) contains also the processes scaling with the dynamical Stark shift $U_0 = g^2/\Delta_a$, where g is the cavity vacuum Rabi frequency and $\Delta_a = \omega_L - \omega_a$ the detuning between the laser and atomic transition frequency. These processes are here small but accounted for in the numerical simulations [31].
- [40] K. Jain, F. Bouchet, and D. Mukamel, *J. Stat. Mech.* (2007) P11008.
- [41] P. Domokos, P. Horak, and H. Ritsch, *J. Phys. B* **34**, 187 (2001).
- [42] See Supplemental Material at <http://link.aps.org/supplemental/10.1103/PhysRevLett.117.083001> for the quenches along path B in Fig. 1 and the derivation of the mean-field FPE and the Vlasov equation.
- [43] S. B. Jäger, S. Schütz, and G. Morigi, *Phys. Rev. A* **94**, 023807 (2016).
- [44] O. S. Mishina, *New J. Phys.* **16**, 033021 (2014).
- [45] M. J. Bhaseen, J. Mayoh, B. D. Simons, and J. Keeling, *Phys. Rev. A* **85**, 013817 (2012).
- [46] B. Olmos, I. Lesanovsky, and J. P. Garrahan, *Phys. Rev. Lett.* **109**, 020403 (2012).
- [47] D. Nagy and P. Domokos, *Phys. Rev. Lett.* **115**, 043601 (2015).
- [48] M. Kulkarni, B. Öztöp, and H. E. Türeci, *Phys. Rev. Lett.* **111**, 220408 (2013).
- [49] F. Piazza and P. Strack, *Phys. Rev. A* **90**, 043823 (2014).
- [50] K. Baumann, C. Guerlin, F. Brennecke, and T. Esslinger, *Nature (London)* **464**, 1301 (2010); F. Brennecke, R. Mottl, K. Baumann, R. Landig, T. Donner, and T. Esslinger, *Proc. Natl. Acad. Sci. U.S.A.* **110**, 11763 (2013).
- [51] M. Wolke, J. Klinner, H. Keßler, and A. Hemmerich, *Science* **337**, 75 (2012); J. Klinder, H. Keßler, M. Wolke, L. Mathey, and A. Hemmerich, *Proc. Natl. Acad. Sci. U.S.A.* **112**, 3290 (2015).